RSC Advances

PAPER

View Article Online
View Journal | View Issue

Cite this: *RSC Adv.*, 2016, **6**, 39275

Semi-transparent, conductive thin films of electrochemical exfoliated graphene†

Z. M. Marković,*[ab] M. D. Budimir,[b] D. P. Kepić,[b] I. D. Holclajtner-Antunović,[c] M. T. Marinović-Cincović,[b] M. D. Dramićanin,[b] V. D. Spasojević,[b] D. B. Peruško,[b] Z. Špitalský,[a] M. Mičušik,[a] V. B. Pavlović[d] and B. M. Todorović-Marković*[b]

Received 16th February 2016
Accepted 7th April 2016

DOI: 10.1039/c6ra04250c

www.rsc.org/advances

The electrochemical exfoliation of graphite to give one-atom-thick graphene with desirable properties is a green, cost-effective method for high-yield graphene production. This paper presents the results of electrochemical exfoliation of two different graphite precursors under an applied direct current voltage of +12 V. The used characterization techniques (elemental analysis, Fourier transform infrared spectroscopy, X-ray diffraction, X-photoelectron spectroscopy, Raman spectroscopy, field emission scanning electron microscopy and atomic force microscopy) showed that the exfoliated powder is highly functionalized with a low carbon/oxygen content that is similar to graphene oxide. The exfoliated graphene sheets dispersed in *N*,*N*′-dimethylformamide were deposited on ano-discs by vacuum filtration and transferred to glass ceramic substrates. The thermal annealing of the as-deposited films at 600 °C for 30 minutes resulted in an increase in the carbon/oxygen ratio by more than 3 fold and a decrease in the sheet resistance by 25%. The lowest values for the sheet resistance of the annealed graphene thin films were in the range of 0.32 ± 0.04 to 0.84 ± 0.1 kohm sq^{-1} depending on the graphite source that was used.

1. Introduction

Graphene, a one-atom-thick carbon sheet has been attracting the attention of many researchers because of its unique physical, chemical, electrical, mechanical and optical properties.[1] This material is a good candidate for possible electronic applications in many fields: touch screens, flexible displays, printable electronics and solar cells.[2–5] A high-quality graphene monolayer on the wafer scale can be obtained by chemical vapor deposition (CVD) and epitaxial growth.[6–8] However, these techniques are too expensive for the mass production of graphene. Few-layer graphene (FLG) or multi-layer graphene (MLG) consists of a small number (between two and approximately 10) of well-defined, countable, stacked graphene layers of extended lateral dimension either as a free-standing flake or a substrate-bound coating.[9]

One of the possible methods for the low-cost mass production of graphene is the process of graphene exfoliation in liquids by electrochemical, chemical, and sonication-assisted techniques.[10] Graphene can be exfoliated from graphite through ultrasonic treatment in organic solvents such as *N*,*N*′-dimethylformamide (DMF) and *N*-methylpyrrolidone (NMP).[11,12] Chemical exfoliation based on Hummers' method can produce graphene derivatives in a large quantity.[13] In the presence of strong oxidants, the aromatic carbon network is oxidized with the creation of hydroxyl, carboxyl and epoxy moieties.[14–16] The produced graphene oxide (GO) can then be reduced back to conductive reduced graphene oxide. However, the electronic properties of this reduced graphene oxide are poor compared with pristine graphene.

The electrochemical exfoliation of graphite to give graphene is a facile, mild, low-cost environmentally-friendly and sustainable approach compared with the methods mentioned above. For successful graphite exfoliation several different electrolytes can be used: ionic liquids, acids and high-temperature molten salts.[10,17–23] Sodium dodecyl sulfate as well as Na^+/dimethylsulfoxide complexes, can be used as an electrolyte for graphene synthesis.[24,25] Recently, Coros *et al.* have demonstrated that the size of graphene flakes and the exfoliation/oxidation level can be controlled by changing the applied bias and electrolyte concentration.[26] The main advantage of the electrochemical exfoliation of graphite is the easy processing of graphene and functionalized graphene. However,

[a]*Polymer Institute, Slovak Academy of Sciences, Dubravska cesta 9, 84541, Bratislava, Slovakia. E-mail: zm25101967@yahoo.com; zoran.markovic@savba.sk; Tel: +421 381 11 3408582*

[b]*Vinča Institute of Nuclear Sciences, University of Belgrade, P. O. B. 522, 11001, Belgrade, Serbia. E-mail: biljatod@vinca.rs*

[c]*Faculty of Physical Chemistry, University of Belgrade, Studentski trg 12-16, 11158, Belgrade, Serbia*

[d]*Faculty of Agriculture, Department of Agricultural Engineering, University of Belgrade, Nemanjina 6, Zemun, 11080, Serbia*

† Electronic supplementary information (ESI) available. See DOI: 10.1039/c6ra04250c

this method has some disadvantages such as the use of hazardous reagents (*e.g.* ionic liquids, phosphoric acid, lithium perchlorate, and 3-(aminopropyl)triethoxysilane), additional steps, high voltages and multi-layer graphene formation.

The electrical properties, especially the sheet resistance of synthesized graphene thin films can be changed over a very broad range depending on different parameters: the production method, film thickness, lateral size of the graphene sheets, thin film optical transmittance, substrates used, *etc.* Table S1 (in the ESI†) lists the values of the sheet resistances of thin films depending on the graphene production method, lateral sizes of graphene sheets and transmittances.[27–36] The sheet resistances of electrochemically exfoliated graphene films are low compared with graphene produced by other methods. Only expensive CVD methods produce graphene with better opto-electronic properties.

In this paper, the structural and electronic properties of graphene produced by the exfoliation of two different graphite sources are compared. Highly oriented pyrolytic graphite (HOPG) is a highly pure and ordered form of synthetic graphite. It is characterized by superior alignment of the individual graphite crystallites. A spectroscopic graphite electrode (SPG) is produced by carbonizing mixed coke substances with binding pitch at 1000 °C in a baking furnace. When this carbon is graphitized in an electric furnace at 3000 °C, the amorphous carbon body takes on the structure of crystalline graphite. The resulting individual graphite crystallites are not aligned with each other. We expected that the graphene produced by the exfoliation of HOPG would have much better electronic properties than with exfoliated graphene from SPG, because of the higher quality of the starting precursor.

In this work, we electrochemically exfoliated a spectroscopic graphite rod and highly oriented pyrolytic graphite in ammonium persulfate ($(NH_4)_2(SO_4)_2$) with a direct current (DC) voltage of +12 V. The exfoliated graphite was dispersed in DMF. Graphene thin films were deposited by vacuum filtration on ano-disc inorganic membranes and later were successfully transferred to glass ceramic substrates. The obtained highly conductive graphene films consist of stacked graphene sheets with lateral size larger than 12 μm. The used ano-disc filters enabled the facile transfer of graphene thin films to the desired substrates. The lowest sheet resistances of the resulting graphene films are 0.84 ± 0.1 and 0.32 ± 0.04 kohm sq^{-1} depending on the graphite source that was used.

2. Experimental section

2.1. Preparation of graphene dispersion and graphene thin films

The electrochemical exfoliation of graphite was performed in a two-electrode system placed in a electrolyte (ammonium persulfate, Sigma Aldrich, in the text as APS). As graphite precursors, spectroscopic graphite rods (in the text as SPG, Ringsdorff-Werke, SGL Carbon, Germany, purity of 99.999%) and HOPG (20 × 50 × 0.6 mm, produced at the Vinča Institute of Nuclear Sciences, Serbia) were used. As a counter electrode, platinum wire was used. A direct current voltage of +12 V was applied. The electrolyte solution was prepared by dissolving $(NH_4)_2SO_4$ in water (a concentration of 0.1 M). The exfoliation process lasted from 2 to 24 hours. The mass of the exfoliated product was up to 12 g per day. The exfoliated SPG powder and HOPG (in the text – as EG and EHOPG, respectively) were washed with 5 L of MilliQ water using a coarse filter paper with a pore size of 15 microns. APS and small-size graphene flakes were washed. EG and EHOPG were dried at 100 °C for 24 hours in air. During electrolysis, SPG undergoes significant fragmentation. The detached fragments are no longer charged; thus they do not further exfoliate. On the other hand, HOPG maintains its integrity throughout the entire process. The only visible change is its expansion at the end of process. Then, EHOPG is milled in an agate mortar.

EG and EHOPG powders were dispersed in *N*,*N*-dimethylformamide by ultrasonication for 5 min. The DMF dispersion was allowed to settle for 2 days. Then, this dispersion was centrifuged at 6500 rpm for 30 min. The yields of multi-layer graphene produced by the exfoliation of SPG and HOPG were 76 ± 5% and 42 ± 7%, respectively. The supernatant was used for the deposition of thin films and colloidal characterization. The thin films were deposited by vacuum filtration on ano-disc inorganic membranes with a pore size of 200 nm (Whatman filters). The thickness of the thin films depends on the volume of the graphene/DMF dispersion used. The deposited graphene thin films were transferred to glass ceramic substrate using a 0.5 M NaOH solution for ano-disc etching. Finally films of EG and EHOPG were annealed at 600 °C in a Torvac vacuum furnace (Torvac, UK) for 30 min (in the text – as AEG600 and AEHOPG600, respectively). Powders of EG and EHOPG were also annealed at 100 °C, 300 °C and 800 °C in the Torvac vacuum furnace (Torvac, UK) for 30 minutes (in the text – as AEG100, AEG300, AEG800, AEHOPG100, AEHOPG300 and AEHOPG800, respectively).

2.2. Characterization of exfoliated graphite, HOPG and graphene thin films

The elemental analysis of graphene sheets exfoliated from SPG and HOPG were conducted with a Leco CHNS 628 elemental analyzer. The precision range for the detector is C (0.01 mg or 0.5% RSD whichever is higher), H (0.05 mg or 1% RSD whichever is higher), N (0.02 mg or 0.5% RSD whichever is higher) and S (0.005 mg or 1% RSD whichever is higher).

XPS was performed using a Thermo Scientific K-Alpha XPS system (Thermo Fisher Scientific, UK) equipped with a micro-focused, monochromatic Al Kα X-ray source (1486.6 eV). An X-ray beam of 400 mm in size was used at 6 mA × 12 kV. The spectra were acquired in the constant analyzer energy mode with a pass energy of 200 eV for the survey. Narrow regions were collected with a pass energy of 50 eV. Charge compensation was achieved with the system flood gun that provides low energy electrons (~0 eV) and low energy argon ions (20 eV) from a single source. Thermo Scientific Avantage software, version 5.952 (Thermo Fisher Scientific), was used for the digital acquisition and data processing. Spectral calibration was determined by using the automated calibration routine and the

internal Au, Ag and Cu standards supplied with the K-Alpha system.

The surface composition (in atomic%) was determined by considering the integrated peak areas of the detected atoms and their respective sensitivity factors. The fractional concentration of a particular element A was computed using:

$$\% A = \frac{I_A/s_A}{\sum(I_n/s_n)} \times 100\% \quad (1)$$

where I_n and s_n are the integrated peak areas and the Scofield sensitivity factors corrected for the analyzer transmission, respectively.

The Fourier transform infrared spectroscopy (FTIR) spectra of the exfoliated graphene sheets were measured at room temperature in the spectral range from 400 to 4000 cm^{-1} on a Nicollet 380 FT-IR, Thermo Electron Corporation spectrometer operating in ATR mode.

X-ray diffraction (XRD) patterns were measured using a Rigaku Smart Lab diffractometer in a 2θ range from 5° to 70° and were counted at 0.7° min^{-1} in 0.1° steps.

Raman spectra of the graphene thin films were obtained by DXR Raman microscope (Thermo Scientific) using a 532 nm excitation line with a power of 5 mW. The spectral resolution was 1 cm^{-1}. The acquisition time was 10 × 10 s. The Raman spectra were recorded at room temperature.

The morphology of EG and EHOPG was characterized by scanning electron microscopy (SEM, JEOL JSM-6390LV). The samples for SEM analysis were pressed on carbon tape and recorded at room temperature.

The morphology and lateral size of the exfoliated sheets were determined by field-emission scanning electron microscopy (FESEM Magellan 400L XHR, FEI Company). Prior to FESEM recordings, a small amount of the sample was dispersed in hexane and placed dropwise onto a holey carbon support grid. Changes in the microstructure and morphology of graphene thin films that were deposited on a glass ceramic substrate were recorded by a field-emission scanning electron microscope (FESEM Magellan 400L XHR, FEI Company) and an atomic force microscope (AFM-Quesant, Ambious Technology, USA). The AFM was operated in tapping mode at room temperature.[37] The AFM measurements were performed in air using a silicon T-shaped cantilever with a spring constant of 40 N m^{-1} on square areas of 1 μm × 1 μm. All images were obtained at 1 Hz, with a 512 × 512 image resolution over different square areas. Gwyddion software was used to measure the lateral and height sizes of graphene sheets.[38]

The optical transmittance of graphene thin films deposited on glass ceramic substrate was measured at 550 nm with a UV-vis spectroscope monitoring a wavelength range of 300–1350 nm using an Avantes UV-vis spectrophotometer.

The sheet resistance of the annealed graphene thin films deposited on a glass ceramic substrate was measured by the four-point probe method at room temperature. The sheet resistance was measured on 5 different places on the thin film surface, and the average was taken.

3. Results and discussion

3.1. Elemental analysis of exfoliated graphite rod and HOPG

The elemental analysis of the EG, EHOPG, EG100, EG300, AEG800, AEHOPG100, AEHOPG300 and AEHOPG800 samples is presented in Table 1.

The results of the elemental analysis show that hydrogen, nitrogen and sulfur remain in the powders regardless of the annealing temperature. However, the oxygen content reduces significantly. The elemental analysis shows that the carbon/oxygen (C/O) ratios are 5.34 for EG and 2.21 for EHOPG. These ratios indicate that a very strong oxidation of the exfoliated graphene sheets took place during the electrochemical procedure and that the obtained values are similar to those obtained for reduced graphene oxide.[39,40] After annealing at 100 °C, 300 °C and 800 °C, C/O ratio is 6.06, 8.29 and 13.89, respectively for EG. As for EHOPG sample, C/O ratios are the following: 4.59, 6.28 and 13.47, respectively. These results indicate that thermal annealing removes oxygen functional groups very effectively.

3.2. XPS analysis of exfoliated graphite rod and HOPG

Fig. 1 shows the XPS spectra of EG and EHOPG before and after annealing at 600 °C. The XPS survey spectra presented in Fig. 1(a, c, e and g) demonstrate the clear presence of sulfur, carbon, nitrogen and oxygen. After the deconvolution of the C 1s peak, the presence of the following carbon bonds is established: sp^2, sp^3, C–O, C═O, O–C═O and π–π* – Fig. 1(b, d, f and h). Tables 2 and 3 present the contents of the elements as an atomic percentage (at%) and the values of the characteristic bonds detected in EG, EHOPG AEG600 and AEHOPG600, respectively.

The carbon and oxygen content are similar in the EG and EHOPG samples. However, the nitrogen and sulfur contents are several times larger in EHOPG, because of the prolonged exposure to negative ions during electrolysis. However, the main difference between the EG and EHOPG samples is the content of C–O and C═O bonds. In the EHOPG sample, the carbon atoms are mainly attached to oxygen *via* a single bond (25.8%), whereas in the EG sample, the carbon atoms predominantly form double bonds with the oxygen atoms

Table 1 Elemental analysis: the content of elements in (%) in the EG, EHOPG EG100, EG300, EG800, EHOPG100, EHOPG300 and EHOPG800 samples

Sample	C (%)	H (%)	N (%)	S (%)	O (%)
EG	81.8	0.8	0.5	1.5	15.3
EHOPG	66.1	2	0.2	1.8	29.9
EG100	84.8	0.6	0.2	0.4	14.0
EG300	87.9	0.4	0.1	0.3	10.6
EG800	91.7	0.4	0.1	0.3	6.6
EHOPG100	80.4	1.5	0.2	0.4	17.5
EHOPG300	84.8	1.2	0.1	0.4	13.5
EHOPG800	91.6	1.1	0.1	0.4	6.8

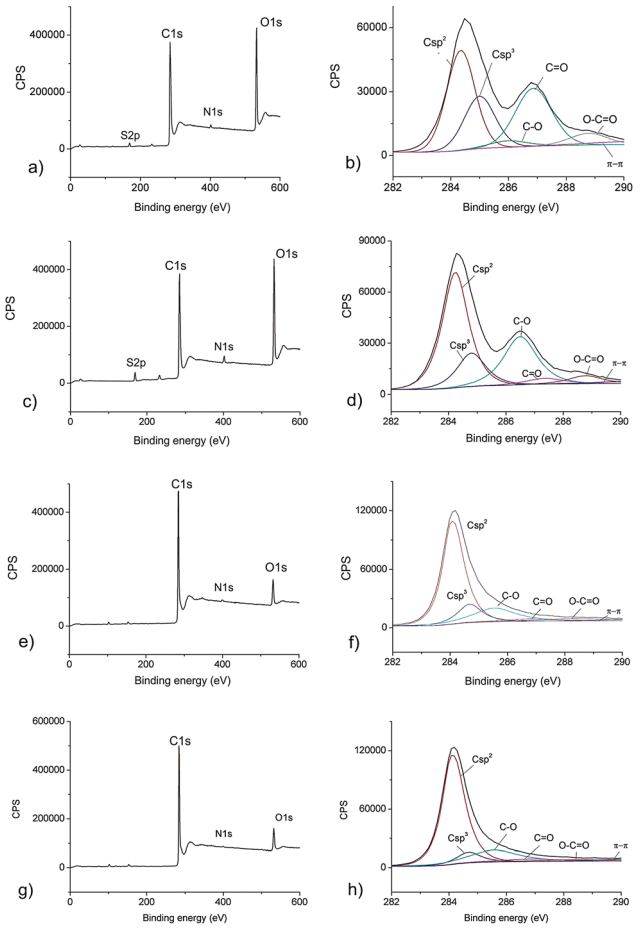

Fig. 1 (a) XPS survey spectrum of EG; (b) the fitted XPS spectrum of the C 1s peak of the EG sample; (c) the XPS survey spectrum of EHOPG; (d) the fitted XPS spectrum of the C 1s peak of the EHOPG sample; (e) the XPS survey spectrum of AEG600; (f) the fitted XPS spectrum of the C 1s peak of the AEG600 sample; (g) the XPS survey spectrum of AEHOPG600 and (h) the fitted XPS spectrum of the C 1s peak of AEHOPG600.

Table 2 XPS data of the elements detected in the EG, EHOPG, AEG600 and AEHOPG600 samples (at%)

Name	EG	EHOPG	AEG600	AEHOPG600
C 1s	77.2	70.7	89.2	91.1
O 1s	21.7	24.6	9.7	8.3
N 1s(C–N/N$^+$)	0.7(0.2/0.5)	2.4(0.3/2.1)	1.1(1.1/0)	0.5(0.5/0)
S 2p	0.4	2.3	—	—

(27.26%). The values of the other carbon bonds (sp^2, sp^3, O–C═O and π–π*) are nearly identical in the two samples.

The XPS results showed that during the electrochemical exfoliation of two different graphite sources, a very strong oxidation of the exfoliated graphene sheets occurred. The efficient intercalation of sulfate ions and the electrochemical oxidation result in a large number of functional groups attached to the surfaces and edges of the basal planes of EG and EHOPG. This is confirmed by the presence of the S 2p peak centered at

Table 3 XPS data of the characteristic bonds detected in the EG, EHOPG, AEG600 and AEHOPG600 samples (at%)

Name	Binding energy (eV)	EG	EHOPG	AEG600	AEHOPG600
C 1s sp^2	284.38	48.5	48.5	59.4	66.8
C 1s sp^3	284.98	11.84	15.3	11.7	7.1
C 1s C–O	286.08	3.4	25.8	19.2	15.8
C 1s C═O	286.88	27.3	3.5	2.7	3.9
C 1s O–C═O	288.78	5.6	4.3	3.2	2.8
C 1s π–π*	290.48	6.5	2.7	3.9	3.6

~169 eV corresponding to sulfates/sulfonates.[41] In the case of EG and EHOPG a peak centered at 401.5 eV corresponding to C–NH_3^+/NH_4^+ was also detected.[42] As we can see from Table 2 the amount of quaternized ammonium is very similar to the amount of sulfate indicating some interaction between these two groups. We suppose that the presence of ammonium is a consequence of the APS that remained on the surface.

Tables 2 and 3 and Fig. 1(e–h) present the elemental content detected in the AEG600 and AEHOPG600 samples. As seen from these tables the carbon content is significantly increased in both samples, whereas the oxygen content is reduced significantly (nearly 2 and 3 times for AEG600 and AEHOPG600, respectively). The main effect of the thermal annealing is an increase in the carbon/oxygen ratio and it equals 9.2 (AEG600) and 11 (AEHOPG600). This is attributed to the restacking of the graphene sheets after annealing and can be a cause of the increase in the electrical conductivity of both types of graphene thin films

The carbon sp^2 content increased nearly 40% in both samples. Additionally, the oxygen is not bonded to the carbon atoms in AEG600 *via* double bonds, as it is in EG. After thermal annealing, AEG600 and AEHOPG600 have very similar chemical composition and types of bonds.

The oxygen functional groups in the graphene basal plane in graphene oxide consist of epoxy and hydroxyl molecules, and the edges can comprise carboxyls, anhydrates, lactones, phenols, lactols, pyrones, and ketones.[15] Therefore, XPS indicate that the functional groups on the EG graphene sheets are located primarily on the edges. In contrast, the basal plane and edges of the larger EHOPG graphene sheets are functionalized. This conclusion is supported by AFM images of EHOPG graphene on which huge defects in the HOPG structure can be readily noticed (presented in Section 3.6).

3.3. FTIR spectra of EG and EHOPG

The attenuated total reflectance (ATR) FTIR spectra of the as-deposited EG and EHOPG thin films are presented in Fig. 2a (curves 1 and 2). The FTIR-ATR spectra of both material show two small peaks at 2830 and 2920 cm^{-1} which stem from C–H stretching vibrations. Both of the spectra show a peak at 2520 cm^{-1} that originates from O–H stretching vibrations. The peaks at 1600 and 2170 cm^{-1} indicate skeletal vibrations from unoxidized graphitic domains. The peaks at 1990 and 1720 cm^{-1} indicate the presence of C═O stretching vibrations in the

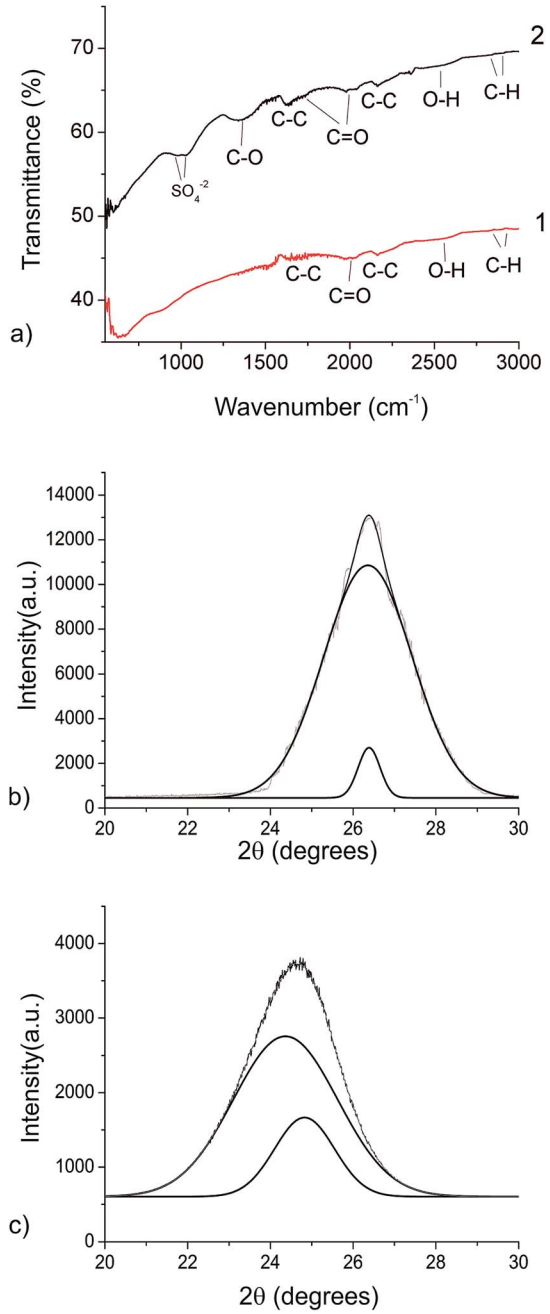

Fig. 2 (a) FTIR-ATR spectra of the as-deposited EG (curve 1) and EHOPG (curve 2) thin films; (b) XRD of the EG and (c) EHOPG powders.

EHOPG thin films – curve 2. As for the EG thin films, the peak at 1990 cm^{-1} indicates the presence of carbonyl groups – curve 1.

The peaks at 1420 and 1050 cm^{-1} stem from C–O stretching vibrations and can be observed only in the EHOPG thin films – curve 2. The peaks at 985 and 1020 cm^{-1} stem from free sulfate ions and can be observed only in the EHOPG sample.

The FTIR spectra of AEG600 and AEHOPG600 thin films are almost identical to those of the EG and EHOPG films. Therefore, the FTIR measurements were not sensitive enough to detect the changes in the structure of the EG and EHOPG samples.

3.4. Determination of number of graphene layers

The XRD analysis was used to determine the number of graphene layers in the precursors and exfoliated materials.

The mean crystallite size (D) was calculated from the full width at half maximum (FWHM) of the XRD peak, using the Debye–Scherrer equation.[26] The interlayer distance (d) was found using the Bragg equation.[43] The average number of graphene layers was obtained by division of the mean crystallite size and the interlayer distance.

Table 4 presents the number of layers (n) and the interlayer distance for the precursors and exfoliated materials.

Fig. 2(b and c) present the fitted XRD spectra of EG and EHOPG. Despite severe oxidation, the obtained exfoliated materials do not contain graphene oxide as characterized by a peak at $2\theta \approx 11°$. The average number of layers was reduced by one order of magnitude. The interlayer spacing has increased by 3 and 7% for EG and EHOPG, respectively.

3.5. Raman spectroscopy of exfoliated graphite and HOPG

Raman spectroscopy is a very powerful tool for the structural investigation of different types of carbon nanomaterials. The most prominent features in the Raman spectra of graphene are the G band appearing at 1582 cm^{-1}, the 2D band at 2700 cm^{-1} and the D band at 1350 cm^{-1}. The G band is associated with the doubly degenerate phonon mode (E_{2g} symmetry) at the Brillouin zone center.[44] In fact, the G band is the only band coming from a normal first-order Raman scattering process in graphene. In contrast, the 2D and D bands originate from a second-order process. It is known that the D band originates from inter-valley double resonance processes, because of the short-range disorder potentials (*e.g.*, adatoms, vacancies and defects),[45] whereas the D′ band originates from the intra-valley double resonance processes induced by long-range disorder (ripples, dislocations and charged impurities).

Representative Raman spectra of the SPG, and AEG600 thin films and the HOPG and AEHOPG600 thin films are presented in Fig. 3. As seen in Fig. 3 we can observe characteristic peaks for graphene in all four of the recorded Raman spectra: the D peak, G peak and the 2D peaks. The D′ peak can be observed only in the HOPG sample (Fig. 3b – curve 1). Depending on the sample the positions of the D, G and 2D peaks differ. Table 5 shows the positions of the D, G, 2D peaks of the SPG and AEG600 thin films; and the HOPG and AEHOPG600 thin films; as well as the corresponding I_D/I_G ratio. Based on the results

Table 4 Number of layers (n) and the interlayer distance (d) of SPG, HOPG, EG and EHOPG

	n	d (nm)	n	d (nm)
SPG	537	0.334	—	—
HOPG	99	0.348	—	—
EG	11	0.347	35	0.346
EHOPG	9	0.373	16	0.367
AEG600	11	0.346	35	0.346
AEHOPG600	9	0.372	16	0.367

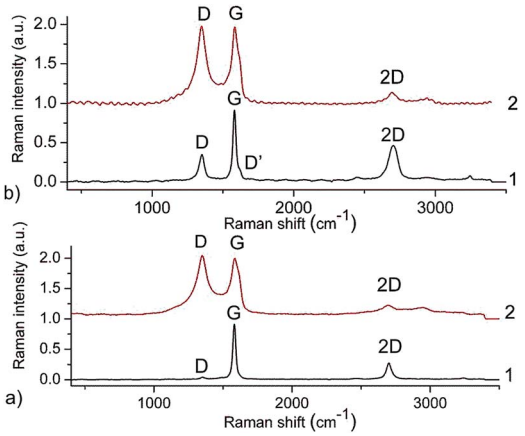

Fig. 3 Raman spectra of (a) HOPG – curve 1, AEHOPG600 – curve 2; and (b) SPG – curve 1, AEG600 – curve 2.

Table 5 Positions of characteristic features of SPG, AEG600, HOPG and AEHOPG600

	D peak position (cm^{-1})	G peak position (cm^{-1})	2D peak position (cm^{-1})	I_D/I_G
SPG	1355.034	1580.665	2701.104	0.36
AEG600	1349.472	1586.071	2693.619	1
HOPG	1351.177	1581.629	2703.032	0.04
AEHOPG600	1351.401	1584.922	2704.22	1.03

presented in Table 5 we can conclude that there is a small upshift of the G peak of both samples (5.4 cm^{-1} (AEG600) and 3.3 cm^{-1} (AEHOPG600)). The upshifts in the G peaks of both samples indicate chemical doping of the exfoliated sheets (p-type doping).

Fig. 4 presents the fitted Raman spectra of the reference samples (SPG and HOPG) and the AEG600 and AEHOPG600 thin films. The G peaks of the thin films were fitted by four Lorentzian peaks (1510, 1580, 1610 and 1620 cm^{-1}) whereas the Raman spectra of the reference samples were fitted with 2 Lorentzian (1580 and 1620 cm^{-1}) peaks. The last three peaks are denoted as P1, P2 and P3 in Fig. 4b and d. As can be seen in Fig. 4b and d (1580 and 1610 cm^{-1}), the fitted Raman spectra exhibit a doublet structure at frequencies close to the singlet E_{2g} peak found in pristine graphite. The lower frequency component is attributed to the carbon vibrations in the interior of the graphite layers (a frequency range from 1580 to 1590 cm^{-1} – P1) whereas the upper frequency component is due to carbon vibration between the bound graphite layers, and adjacent to intercalants (a frequency range from 1600 to 1630 cm^{-1} – P2).[46] The intensity ratio of P1 to P2 can be related to the intercalation stage index n denoting the number of graphitic layers between adjacent intercalate layers.[10] The P3 peak corresponds to the edge defects in graphene (designated as the D′ peak in the graphene Raman spectrum). Based on the fitted spectra of the thin films (Fig. 4b and d) we can determine the intercalation stage index n.

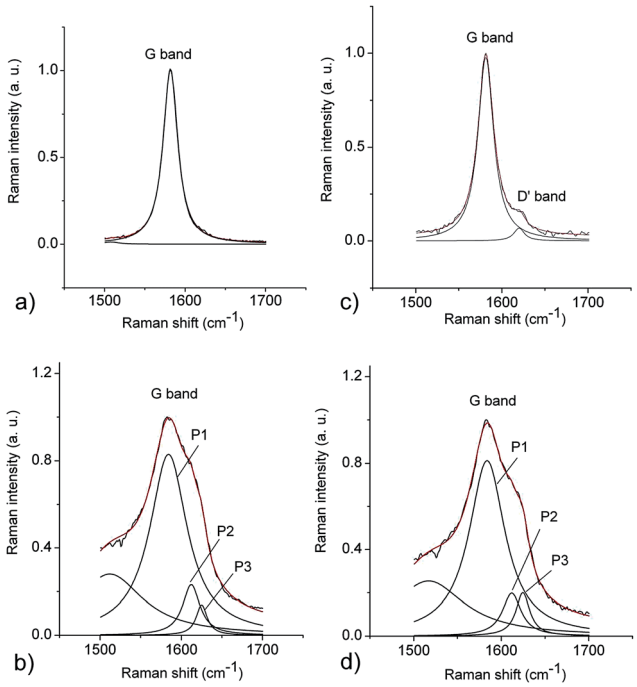

Fig. 4 Fitted Raman spectra of the G band of (a) HOPG, (b) AEHOPG600, (c) SPG, and (d) AEG600.

Therefore, the intercalation stage index for the AEG600 sheets is $n = 11$ whereas for the AEHOPG600 sheets it is $n = 10$. These data show that the basic building block is composed of 11(10) graphene layers and coated with one layer of the intercalated material. The I_D/I_G ratio increased 23.3 times during the processing of HOPG. In contrast, the I_D/I_G ratio increased only 2.8 times during the processing of SPG.

3.6. Surface morphology of EG and EHOPG and annealed graphene thin films

In Fig. 5, AFM, SEM and FESEM micrographs of the EG and EHOPG graphene sheets are presented. Fig. 5(a and b) show low-magnification SEM micrographs of the EG and EHOPG material.

There is a substantial difference in the morphology of the exfoliated powders. In Fig. 5a, it can be observed that exfoliated MLG are separated by distances in the range of 1.5–2 μm (assigned by arrows). There is also a broad distribution in the sheet size (2–12 μm). The EG sheets have many ripples and folded edges throughout the graphene planes. As for EHOPG, it is obvious from Fig. 5b that there are large continuous HOPG sheets with a size of approximately 20 μm. The graphene sheets are flat whereas their edges are etched (shown by arrows in Fig. 5b). Fig. 5c shows a top view AFM image of the few-layer EG with an average lateral size of approximately 4 μm. The maximum lateral size of few-layer EG is 12 μm. From this top view AFM image one can observe that short term electrochemical exfoliation of SPG yields many ripples due to surface cracking and macroscopic deformation of the surface. Fig. 5f shows a top view AFM image of few-layer EHOPG with average

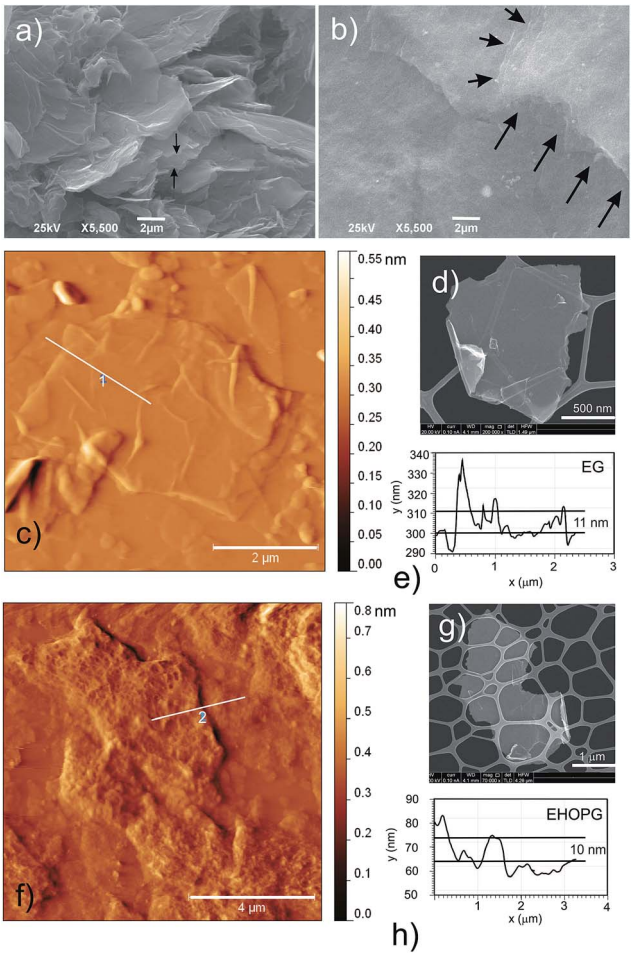

Fig. 5 (a) SEM micrograph of EG; (b) the SEM micrograph of EHOPG; (c) the top view AFM image of the EG sample; (d) the FESEM micrograph of the EG sample; (e) the height profile of a graphene sheet of the EG sample; (f) the top view AFM image of the EHOPG sample; (g) the micrograph of the EHOPG sample; and (h) the height profile of a graphene sheet of the EHOPG sample.

lateral size of approximately 12 μm. This image reveals the etched structure of EHOPG with many holes in the sheet surface. It is reminiscent of a "spider web" structure. The maximum lateral size of the few-layer EHOPG is 20 μm. Based on a statistical analysis conducted on a few AFM images we calculated that average lateral size of the FLG sheets from EHOPG is 3 times larger those from the EG sample.

The average height of an EG sheet is 11 nm whereas that of an EHOPG sheet is 10 nm – Fig. 5e and h.

Fig. 5(d and g) present typical FESEM micrographs of few-layer EG and EHOPG samples. The edges of FLG in both samples are partially folded and have regular shapes.

Therefore, electrochemical exfoliation under selected conditions from both graphite sources yields typical FLG with lateral sizes ranging from 500 nm to 20 μm and an average height of 10 to 11 nm.

Fig. 6 presents the surface morphology of the AEG600 and AEHOPG600 film measured by FESEM and AFM. Both types of graphene thin films are homogeneous and uniform but the lateral size of the FLG exfoliated from HOPG is larger than that exfoliated from the SPG (3 times). The root-mean-square (RMS) of the AEG600 thin films is 14.7 nm whereas that for the AEHOPG600 thin films RMS equals 12.3 nm. The average lateral size of an EG sheet is 4 μm whereas the average lateral size of an EHOPG sheet is 12 μm.

3.7. Optoelectronic properties of FLG

Fig. 7 presents transmittances of the EG, EHOPG, AEG600 and AEHOPG600 thin films as a function of their sheet resistances.

Various parameters can affect the sheet resistances of thin films: the film thickness, substrate, deposition method, lateral size of the graphene sheets, contact resistances between graphene sheets *etc.* The optical thicknesses of the AEG600 and AEHOPG600 thin films (d_{opt}) were calculated using the equation presented in ref. 47.

The main result is that the sheet resistances of the as-deposited films are higher approximately 25% higher than those of the annealed thin films (Fig. 7 – curves 1 and 2). The second major result is that sheet resistances of the AEHOPG thin films are small compared with the AEG thin films. The lowest values for the sheet resistance of the annealed films are 0.32 ± 0.04 and 0.84 ± 0.1 kohm sq^{-1}, as shown in Fig. 7 (curve 3-AEG600 and curve 4-AEHOPG600) whereas the thicknesses of these films are 36 and 34 nm, respectively. Our results (sheet size, sheet resistivity) are better than the results of other groups that used HOPG as a precursor.[20,35] Only Parvez *et al.* using graphite foil as precursor reported better results than ours.[34]

3.8. Discussion

We now consider some aspects of the exfoliation process of the two different graphite sources (SPG and HOPG) in the APS solution. The applied voltage and concentration of the solution were identical. Because of the nature of the graphite precursor,

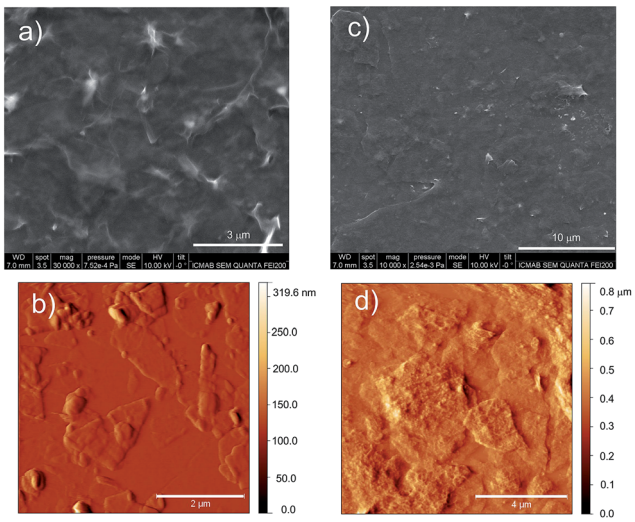

Fig. 6 FESEM micrographs of the AEG600 (a) and AEHOPG600 thin films (c); top view AFM images of the AEG600 (b) and AEHOPG600 thin films (d).

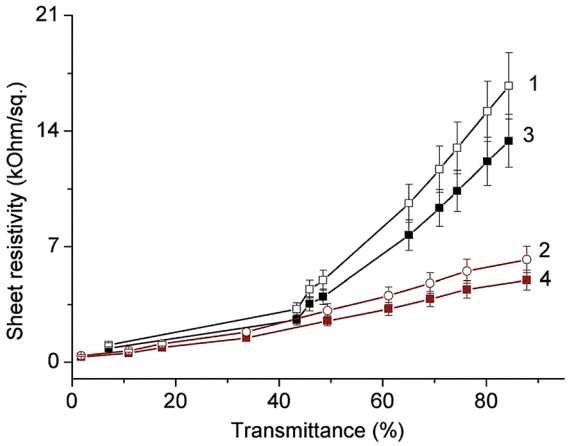

Fig. 7 Transmittance of the EG and AEG600 films (curves 1 and 3) and the EHOPG and AEHOPG600 (curves 2 and 4) thin films as a function of the corresponding sheet resistances.

HOPG exfoliation lasted significantly longer than that for SPG. During electrolysis, SPG fragmented rather rapidly whereas HOPG retained its integrity and electrical contact.

The results presented in this paper clearly demonstrate very small differences in the chemical composition, sp^2 content, p-doping level, intercalation stage index and sheet resistance of the EG and EHOPG films. The major difference is the lateral size of the FLG and EHOPG which is a few times larger.

The spectroscopic graphite rod consists of polycrystalline graphite flakes with different orientation connected by a graphitized binder. HOPG is characterized by the highest degree of three-dimensional ordering. In fact, it belongs to lamellar materials because its crystal structure consists of carbon atoms arranged in stacked parallel layers, and grain boundaries can be seen on the lateral surfaces. The intercalation process preferentially expands the structure at the grain boundaries, edge sites and other intrinsic defects where van der Waals interactions are weak.[48] Sulfate ions penetrate along the grain boundaries in SPG. They promote gas evolution at the corresponding sites. Additionally, they rapidly penetrate into the grain interior and intercalate between the graphene layers. According to the results, one layer of sulfate ions efficiently intercalates every 11 graphene layers on average and promotes exfoliation. In contrast, sulfate ions penetrate into the HOPG interior through edge plane defects. Although the processing time was substantially longer in the case of HOPG, the sulfate ions were unable to homogenously intercalate HOPG. The sole result of the prolonged treatment is the formation of pits in the FLG of the HOPG sample while maintaining a stage index similar to EG.

To improve the exfoliation process, graphite must be pre-treated. Pre-treated graphite should be intercalated with APS to yield stage 1. The Tour method of the intercalation of APS into graphite is very promising.[49] The electrochemical exfoliation of APS-intercalated graphite should lead to the large scale electrochemical production of graphene with large aspect ratios.

4. Conclusions

In this work, we have exfoliated two graphite sources (SPG and HOPG) by applying an electrochemical procedure with a DC voltage of +12 V. We used APS as an electrolyte. Applying different characterization techniques we established that as-deposited HOPG thin films have a much more defective structure (as evidenced by XPS, FTIR, elemental and XRD analyses). Furthermore, the Raman analysis showed that both types of graphene films preserved the intrinsic structure of the sp^2 domain and that every 10(11) graphene layers correspond to one intercalate layer. After annealing, the C/O ratio of both samples increases significantly: 2.59 fold for the EG sample and 3.82 for the EHOPG sample. The EHOPG thin films have lower sheet resistances than the EG films because of the larger lateral size of the graphene sheets, thus leading to smaller number of inter-layer contact resistive paths. The obtained optoelectronic properties of the exfoliated graphene thin films enable the application of these films in electronics.

Acknowledgements

This research was supported by the SASPRO Programme project 1237/02/02-b. The research leading to these results has received funding from the People Programme (Marie Curie Actions) European Union's Seventh Framework Programme under REA grant agreement No. 609427. Research has been further co-funded by the Slovak Academy of Sciences. Research was also supported by the Ministry of Education, Science and Technological Development of the Republic of Serbia (project No. 172003), bilateral project Serbia-Slovakia SK-SRB-2013-0044 (451-03-545/2015-09/07) and VEGA (2/0093/16).

Notes and references

1 K. S. Novoselov, A. K. Geim, S. V. Morozov, D. Jiang, Y. Zhang, S. V. Dubonos, I. V. Grigorieva and A. A. Firsov, *Science*, 2004, **306**, 666.
2 S. Bae, H. Kim, Y. Lee, X. Xu, J. S. Park, Y. Zheng, J. Balakrishnan, T. Lei, H. R. Kim, Y. I. Song, Y. J. Kim, K. S. Kim, B. Özyilmaz, J. H. Ahn, B. H. Hong and S. Iijima, *Nat. Nanotechnol.*, 2010, **5**, 574.
3 P. Blake, P. D. Brimicombe, R. R. Nair, T. J. Booth, D. Jiang, F. Schedin, L. A. Ponomarenko, S. V. Morozov, H. F. Gleeson, E. W. Hill, A. K. Geim and K. S. Novoselov, *Nano Lett.*, 2008, **8**, 1704.
4 M. Choe, B. H. Lee, G. Jo, J. Park, W. Park, S. Lee, W. K. Hong, M. J. Seong, Y. H. Kahng, K. Lee and T. Lee, *Org. Electron.*, 2010, **11**, 1864.
5 X. Wang, L. Zhi and K. Mullen, *Nano Lett.*, 2008, **8**, 323.
6 A. Reina, X. Jia, J. Ho, D. Nezich, H. Son, V. Bulovic, M. S. Dresselhaus and J. Kong, *Nano Lett.*, 2008, **9**, 30.
7 S. Lee, K. Lee and Z. Zhong, *Nano Lett.*, 2010, **10**, 4702.
8 P. W. Sutter, J. I. Flege and E. A. Sutter, *Nat. Mater.*, 2008, **7**, 406.

9 A. Bianco, H. M. Cheng, T. Enoki, Y. Gogotsi, R. H. Hurt, N. Koratkar, T. Kyotani, M. Monthioux, C. R. Park, J. M. D. Tascon and J. Zhang, *Carbon*, 2013, **65**, 1.
10 Z. Y. Xia, S. Pezzini, E. Treossi, G. Giambastiani, F. Corticelli, V. Morandi, A. Zanelli, V. Bellani and V. Palermo, *Adv. Funct. Mater.*, 2013, **23**, 4684.
11 Y. Hernandez, M. Lotya, D. Rickard, S. D. Bergin and J. N. Coleman, *Langmuir*, 2010, **26**, 3208.
12 U. Khan, H. Porwal, A. O'Neill, K. Nawaz, P. May and J. N. Coleman, *Langmuir*, 2011, **27**, 9077.
13 S. Stankovich, D. A. Dikin, R. D. Piner, K. A. Kohlhaas, A. Kleinhammes, Y. Jia and Y. Wu, *Carbon*, 2007, **45**, 1558.
14 A. Lerf, H. Y. He, M. Forster and J. J. Klinowski, *J. Phys. Chem. B*, 1998, **102**, 4477.
15 A. Bagri, C. Mattevi, V. Acik, Y. J. Chabal, M. Chhowalla and V. B. Shenoy, *Nat. Chem.*, 2010, **2**, 581.
16 M. Quintana, A. Montellano, A. E. D. Castillo, G. Van Tendeloo, C. Bittencourt and M. Prato, *Chem. Commun.*, 2011, **47**, 9330.
17 J. Lu, J. X. Yang, J. Wang, A. Lim, S. Wang and K. P. Loh, *ACS Nano*, 2009, **3**, 2367.
18 M. Mao, M. Wang, J. Hu, G. Lei, S. Chen and H. Liu, *Chem. Commun.*, 2013, **49**, 5301.
19 N. Liu, F. Luo, H. Wu, Y. Liu, C. Zhang and J. Chen, *Adv. Funct. Mater.*, 2008, **18**, 1518.
20 C. Y. Su, A. Y. Lu, Y. Xu, F. R. Chen, A. N. Khlobystov and L. J. Li, *ACS Nano*, 2011, **5**, 2332.
21 G. M. Morales, P. Schifani, G. Ellis, C. Ballesteros, G. Martínez, C. Barbero and H. J. Salavagione, *Carbon*, 2011, **49**, 2809.
22 J. Liu, C. K. Poh, D. Zhan, L. Lai, S. H. Lim, L. Wang, X. Liu, N. G. Sahoo, C. Li, Z. Shen and J. Lin, *Nano Energy*, 2013, **2**, 377.
23 H. Huang, Y. Xia, X. Tao, J. Du, J. Fang, Y. Gan and W. Zhang, *J. Mater. Chem.*, 2012, **22**, 10452.
24 M. Alanyalıoglu, J. J. Segura, J. Oró-Solè and N. Casañ-Pastor, *Carbon*, 2012, **50**, 142.
25 M. Zhou, J. Tang, Q. Cheng, G. Xu, P. Cui and L. Qin, *Chem. Phys. Lett.*, 2013, **572**, 61.
26 M. Coros, F. Pogacean, M. C. Rosu, C. Socaci, G. Borodi, L. Magerusan, A. R. Biris and S. Pruneanu, *RSC Adv.*, 2016, **6**, 2651.
27 H. A. Becerril, J. Mao, Z. Liu, R. M. Stoltenberg, Z. Bao and Y. Chen, *ACS Nano*, 2008, **2**, 463.
28 G. Eda, Y. Y. Lin, S. Miller, C. W. Chen, W. F. Su and M. Chhowalla, *Appl. Phys. Lett.*, 2008, **92**, 233305.
29 H. Feng, R. Cheng, X. Zhao, X. Duan and J. Li, *Nat. Commun.*, 2013, **4**, 1539.
30 Y. Hernandez, V. Nicolosi, M. Lotya, F. M. Blighe, Z. Sun, S. De, I. T. McGovern, B. Holland, M. Byrne, Y. K. Gun'Ko, J. J. Boland, P. Niraj, G. Duesberg, S. Krishnamurthy, R. Goodhue, J. Hutchison, V. Scardaci, A. C. Ferrari and J. N. Coleman, *Nat. Nanotechnol.*, 2008, **3**, 563.
31 S. De, P. J. King, M. Lotya, A. O'Neill, E. M. Doherty, Y. Hernandez, G. S. Duesberg and J. N. Coleman, *Small*, 2010, **6**, 458.
32 S. Biswas and L. T. Drzal, *Nano Lett.*, 2009, **9**, 167.
33 J. H. Lee, D. W. Shin, V. G. Makotchenko, A. S. Nazarov, V. E. Fedorov, Y. H. Kim, J. Y. Choi, J. M. Kim and J. B. Yoo, *Adv. Mater.*, 2009, **21**, 4383.
34 K. Parvez, Z. S. Wu, R. Li, X. Liu, R. Graf, X. Feng and K. Müllen, *J. Am. Chem. Soc.*, 2014, **136**, 6083.
35 J. Liu, M. Notarianni, G. Will, V. T. Tiong, H. Wang and N. Motta, *Langmuir*, 2013, **29**, 13307.
36 F. Bausi, A. Schlierf, E. Treossi, M. G. Schwab, V. Palermo and F. Cacialli, *Org. Electron.*, 2015, **18**, 53.
37 B. Todorović Marković, S. Jovanović, V. Jokanović, Z. Nedić, M. Dramićanin and Z. Marković, *Appl. Surf. Sci.*, 2008, **255**, 3283.
38 http://www.gwyddion.net, version 2.42.
39 H. J. Shin, K. K. Kim, A. Benayad, S. M. Yoon, H. K. Park, I. S. Jung, M. H. Jin, H. K. Jeong, J. M. Kim, J. Y. Choi and Y. H. Lee, *Adv. Funct. Mater.*, 2009, **19**, 1987.
40 D. Yang, A. Velamakanni, G. Bozoklu, S. Park, M. Stoller, R. D. Piner, S. Stankovich, I. Junga, D. A. Field, C. A. Ventrice Jr and R. S. Ruoff, *Carbon*, 2009, **47**, 145.
41 *XPS knowledge database, Avantage 5.955*, Thermo Fisher Scientific, UK.
42 G. Beamson and D. Briggs, *High resolution XPS of organic polymers-the scienta ESCA300 database*, Wiley, 1992, pp. 1–306.
43 S. C. Jun, in *Graphene-based energy devices*, ed. A. Rashid bin Mohd Yusof, Wiley-VCH Verlag GmbH&Co. KGaA, 2015, ch. 1: Fundamental of graphene, pp. 1–48.
44 L. M. Malard, M. A. Pimenta, G. Dresselhaus and M. S. Dresselhaus, *Phys. Rep.*, 2009, **473**, 51.
45 A. C. Ferrari, *Solid State Commun.*, 2007, **14**, 47–57.
46 M. S. Dresselhaus and G. Dresselhaus, *Adv. Phys.*, 2002, **51**, 1.
47 S. Eigler, Transparent and Electrically Conductive Films From Chemically Derived Graphene, in *Nanotechnology and Nanomaterials – Physics and Applications of Graphene-Experiments*, ed. Mikhailov, InTech, 2011, pp. 109–134.
48 S. Yang, S. Bruller, Z. S. Wu, Z. Liu, K. Parvez, R. Dong, F. Richard, P. Samor, X. Feng and K. Mullen, *J. Am. Chem. Soc.*, 2015, **137**, 13927.
49 A. M. Dimiev, S. Bachilo, R. Saito and J. M. Tour, *ACS Nano*, 2012, **6**, 7842.